molecules

MDPI

Article

UVC Stokes and Anti-Stokes Emission of $Ca_9Y(PO_4)_7$ Polycrystals Doped with Pr^{3+} Ions

Karol Lemański [1,*], Olha Bezkrovna [1,2], Nadiia Rebrova [1], Radosław Lisiecki [1], Patrycja Zdeb [1] and Przemysław Jacek Dereń [1,*]

[1] Institute of Low Temperature and Structure Research, Polish Academy of Sciences, ul. Okólna 2, 50-422 Wrocław, Poland; o.bezkrovna@intibs.pl (O.B.); n.rebrova@intibs.pl (N.R.); r.lisiecki@intibs.pl (R.L.); p.zdeb@intibs.pl (P.Z.)

[2] Institute for Single Crystals, NAS of Ukraine, Nauky Ave. 60, 61001 Kharkiv, Ukraine

* Correspondence: k.lemanski@intibs.pl (K.L.); p.deren@intibs.pl (P.J.D.)

Abstract: The recent COVID-19 pandemic has made everyone aware of the threat of viruses and the growing number of antibiotic-resistant bacteria. It has become necessary to find new methods to combat these hazards. One tool that could be used is UVC radiation, i.e., 100–280 nm. Currently, the available sources of this light are mercury vapor lamps. However, the modern world requires more compact, mercury-free, and less energy-consuming light sources. This work presents the results of our research on a new material in which efficient UVC radiation was obtained. Here, we present the results of research on $Ca_9Y(PO_4)_7$ polycrystals doped with Pr^{3+} ions prepared using the solid-state method. The absorption, excitation, emission, and emission decay profiles of praseodymium(III) ions were measured and analyzed. The upconversion emission in the UVC region excited by blue light was observed. Parameters such as energy bandgap, refractive index, and thermal stability of luminescence were determined. The studied phosphate-based phosphor possesses promising characteristics that show its potential in luminescent applications in future use in medicine or for surface disinfection.

Keywords: spectroscopy; phosphates; praseodymium; UVC upconversion emission; polycrystals

Citation: Lemański, K.; Bezkrovna, O.; Rebrova, N.; Lisiecki, R.; Zdeb, P.; Dereń, P.J. UVC Stokes and Anti-Stokes Emission of $Ca_9Y(PO_4)_7$ Polycrystals Doped with Pr^{3+} Ions. *Molecules* **2024**, *29*, 2084. https://doi.org/10.3390/molecules29092084

Academic Editor: Pradip K. Bhowmik

Received: 29 February 2024
Revised: 2 April 2024
Accepted: 25 April 2024
Published: 1 May 2024

1. Introduction

UVC radiation (100–280 nm) can successfully inactivate microbes and viruses [1], better than UVB (280–315 nm) or UVA (315–400 nm) light. Phosphors capable of emitting light in the UVC range could have a wide range of medical applications, from self-cleaning surfaces to various medical procedures [2–5], e.g., to sterilize surgical equipment, room disinfection as well as air and water, which is due to the fact that UV sterilization helps to eliminate dangerous pathogens in many public places, e.g., hospitals, workplaces, schools, or airports.

An important issue for obtaining UVC radiation is the choice of host matrix and activator. Rare-earth elements are most often used as an activator. Among them, Pr^{3+} has attracted much attention. Praseodymium(III) has two electrons in the 4f subshell, well shielded by other subshells from the influence of the crystal field, which is characteristic of all lanthanides (Ln). Because of this, the lanthanides in various crystalline compounds possess stable spectroscopic properties. The luminescence of Pr^{3+} ions can be characterized by many colors from near-ultraviolet and blue to infrared range [6–14]. Most often, blue or red emissions dominate, which mainly occurs, respectively, from the $^3P_0$ or $^1D_2$ energy levels to the ground state $^3H_4$. Also, in some hosts doped with Pr^{3+} ions, a strong 5d→4f emission in the UVC range is observed [1,15–17].

In recent years, the accommodation of rare-earth elements in phosphate-based hosts has been widely studied in connection with the luminescent properties they exhibit. The

crystallographic properties of phosphates favor this doping. Phosphates have a lot of applications [18–20]. They are also widely used in the healthcare industry. These compounds are present naturally in human teeth and bones, and they are used in the manufacturing of medicines for these organs [21–23]. They are also used in toothpaste as a polishing agent and to enable the free flow of the paste through a tube. Another important characteristic of phosphates is their prevalence in living organisms. Calcium phosphates are also added to animal feed [20,24,25]. Therefore, we hope that future biocompatibility testing of our best phosphate material will demonstrate its potential for medical applications [19,26].

Calcium phosphate $Ca_9Y(PO_4)_7$ is also a potentially good matrix for doping lanthanide ions in it to obtain efficient luminescence [27–31]; however, the available scientific literature on this matrix is still quite modest. This material is well suited for doping with lanthanide ions, e.g., because the trivalent lanthanide ions are well matched in structure to yttrium ions in terms of good ionic size and valence match. $Ca_9Y(PO_4)_7$ also has a sufficiently large energy gap and an appropriate position of the 5d level that allows Stokes and anti-Stokes emission of Pr^{3+} ions to occur.

In the context of the UVC upconversion, phosphates, despite their high phonon energies [32], which increase the nonradiative multi-phonon relaxation (MPR) rate, can be chosen for the study due to two main advantages. First of all, they possess a wide bandgap that allows for UVC emissions to be observed. Second, some rare-earth doped phosphates also exhibit a significant UV/VIS branching ratio, which can be attributed to small shifts of the parabolas of the 5d vs.4f electronic configuration [17].

The objective of our work was to test the ability of Pr^{3+}-doped $Ca_9Y(PO_4)_7$ phosphate (CYPO) to demonstrate UVC upconversion emission when excited by a blue light. The structure of $Ca_9Y(PO_4)_7$ is a derivative of the structure of $Ca_3(PO_4)_2$. The prevalence of calcium phosphates in the human body makes the derivatives of $Ca_3(PO_4)_2$ highly biocompatible. The undoped CYPO matrix does not exhibit intrinsic luminescence, which could interfere with the luminescence of possible rare-earth activator ions. Thus, $Ca_9Y(PO_4)_7$ doped with Pr^{3+} ions is a promising candidate to obtain the emission in the UVC range induced by the upconversion processes. This feature can later be used in the production of UVC LEDs to destroy viruses and bacteria. The obtained phosphors possess remarkable luminescent properties and high chemical stability and are relatively cheap.

Similar matrices of calcium phosphates were investigated with several doped lanthanides like Eu^{3+}, Dy^{3+}, Pr^{3+}, and Gd^{3+} ions [16,17,27,31,33–37]. These compounds possess interesting crystal structures and, thus, are often investigated by doping lanthanide ions, which exhibit various spectroscopic properties, which mainly depend on the different dopants and other factors, like crystal symmetry, temperature, or pressure. Among the suggested applications, $Ca_9Y(PO_4)_7$ doped with Eu^{3+}, Tm^{3+}, and Dy^{3+} may be promising candidates for light-emitting diodes [27,29]. Additionally, the $Ca_9Y(PO_4)_7$:Tm^{3+},Yb^{3+} phosphor has potential application as an efficient luminescent thermometer in the temperature range of 323–823 K [30]. Based on the structure of $Ca_3(PO_4)_2$, the structure of these phosphates was also studied with the direct entry of doped rare-earth ions into the structure as $Ca_9RE(PO_4)_7$ (where RE is a rare-earth ion, in this case, Nd, Gd, or Dy) [38].

F. Piccinelli et al. investigated a similar whitlockite-like crystal structure of $Ca_9Lu(PO_4)_7$ phosphate, also doped with Pr^{3+} ions. In this case, four crystal sites can be occupied by RE^{3+} ions, but, e.g., Eu^{3+} or Pr^{3+} doped ions prefer to occupy two and three sites, respectively [35]. Camardello et al. studied $Ca_9R^{3+}(PO_4)_7$ (R^{3+} = Al, Ga, Sc, Lu, Y, Gd, La) phosphates doped with Ce^{3+} and Pr^{3+} ions [17]. They discovered that the optical properties are independent of the RE^{3+} cations, which was connected with the preferential occupation of the eight-coordinated calcium site. Chien-Hao Huang et al. showed the UV luminescence of $Ca_9Y(PO_4)_7$, while doped with 0.2% Pr^{3+}, under excitation at 172 nm. In this work, the authors claim that Pr^{3+} ions are expected to occupy the Y^{3+} ions sites [28].

Despite several works describing the properties of $Ca_9Y(PO_4)_7$:Pr^{3+}, none of them present the luminescent analysis of $Ca_9Y(PO_4)_7$ for various concentrations of doped praseodymium in such a broad way. In this work, we present the spectroscopic study of

$Ca_9Y(PO_4)_7$ polycrystals doped with Pr^{3+} ions, with the results of the UVC upconversion emission discovered for the first time in this crystal host.

The investigated phosphors are suitable as materials that are more compact and less energy-consuming light sources because they are polycrystalline powder materials; thus, a small amount of them is enough to obtain the appropriate effect. Moreover, the fact that these materials exhibit luminescence in the UVC range, not only through Stokes emission but also through anti-Stokes emission, significantly reduces the potential costs of such a device, as this emission could be excited by radiation in the visible range matched to the wavelength of commonly used blue LEDs.

2. Results and Discussion

2.1. Structure Analysis

Calcium yttrium heptaphosphate $Ca_9Y(PO_4)_7$ (ICSD: 236034) possesses a crystallographic structure in which there are as many as seven crystallographic positions (sites) for cations, four for Ca^{2+} ions and three for Y^{3+}. The space group is trigonal *R3c* (161). The cell parameters are a = 10.4400(5) Å c = 37.3646(4) Å, a/b = 1.0000 b/c = 0.2794 c/a = 3.5790; V = 3526.89(34) $Å^3$ and Z = 6 [39]. Due to the presence of yttrium (Y^{3+}) ions, which both in terms of charge matching and ionic size are similar to doped lanthanide ions, they are located in the crystal structure without creating defects compensating for the electric charge. The visualization of the unit cell of the measured crystal is shown in Figure 1.

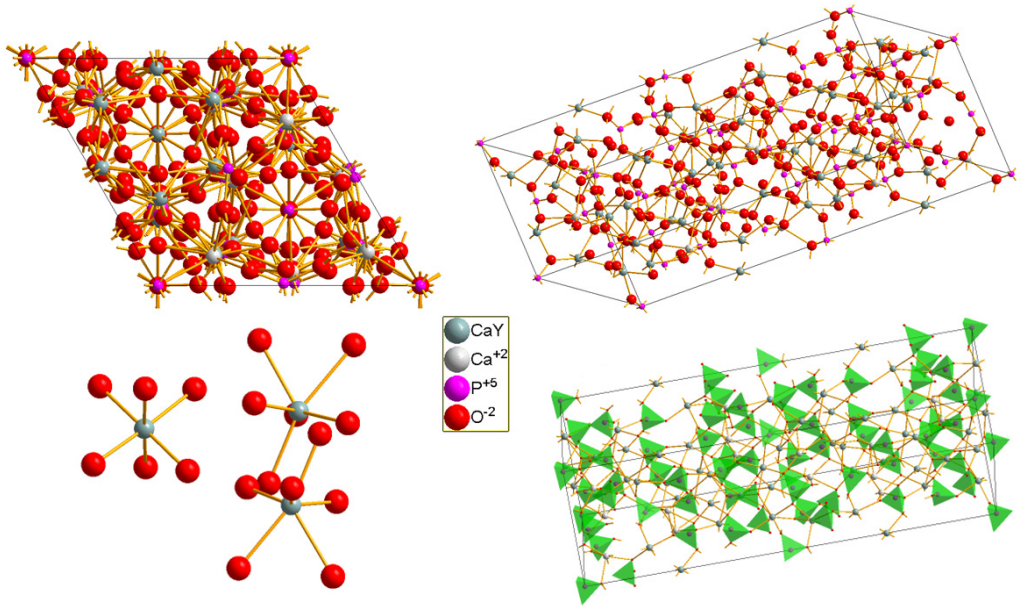

Figure 1. Visualization of the $Ca_9Y(PO_4)_7$ crystal structure.

Calcium(II) ions in the CYPO crystal structure can be found in four sites, while yttrium(III) ions, and praseodymium ions, can be found in three crystallographic positions. These positions are shared with calcium ions. Detailed metal–ligand distance data can be found in Table S1. There are four crystallographic positions for calcium in the investigated structure, three of which are related to the positions of yttrium. Large Pr^{3+} ions should preferentially occupy the eight-coordinated site in this structure [17]. Y^{3+} ions are located in three crystallographic positions, two with eight coordinations, which have metal–oxygen distances very close to each other, and one position with a coordination of six. Therefore, the doped Pr^{3+} ions would mainly occupy the Y1 and Y2 sites which are coordinated by eight oxygen ligands.

Figure 2 shows the XRD spectra of pure and Pr^{3+} doped CYPO. All patterns could be indexed based on the trigonal structure SG: *R3cH* (ICSD No. 236034). Some reflections in the XRD patterns belong to the Y_2O_3 (ICSD 96-720-5918) impurity and are marked in

Figure 2 by asterisks. The calculated lattice parameters of the samples are presented in Table 1. The results showed that the host lattice slightly expands with increasing activator concentration in the nanoparticles (see Table 1) because the ionic radii of Pr^{3+} are larger than that of Y^{3+} [40].

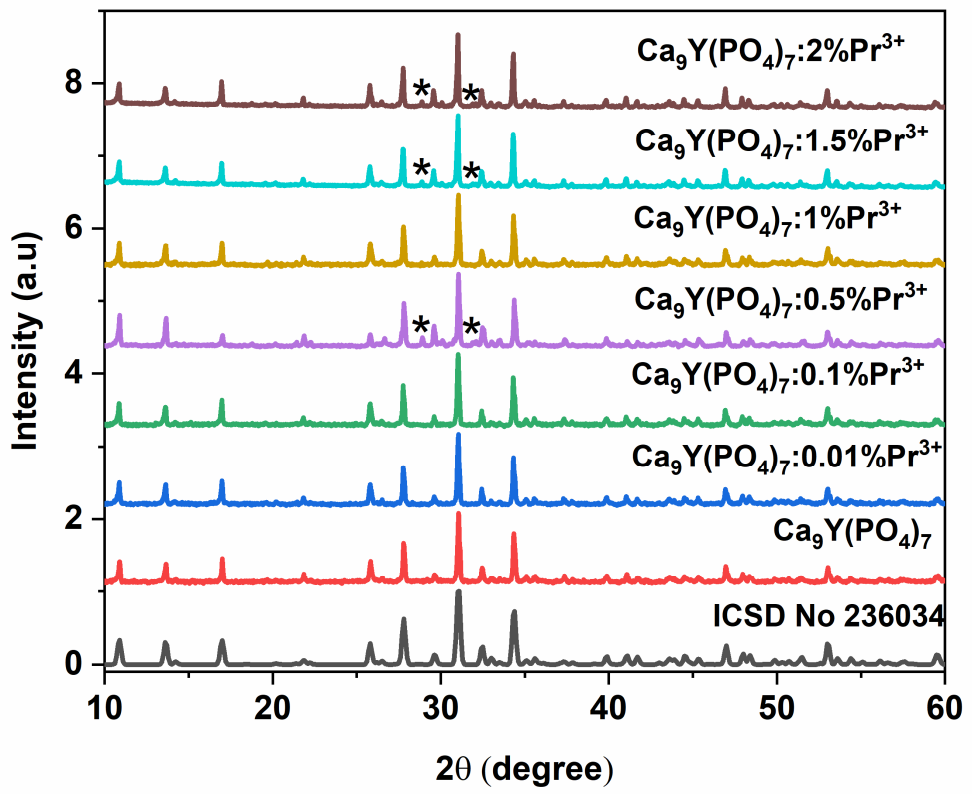

Figure 2. X-ray diffraction patterns of $Ca_9Y_{1-x}Pr_x(PO_4)_7$:Pr^{3+} particles and standard reference of $Ca_9Y(PO_4)_7$. Y_2O_3 impurity reflections are shown by asterisks.

Table 1. Lattice parameters, unit cell volume, and crystallite size of $Ca_9Y_{1-x}Pr_x(PO_4)_7$ ($0 \leq x \leq 0.02$) phosphors calculated from XRD data.

	a (Å)	c (Å)	V (Å^3)	Scherrer Method Size (nm)	W–H Plot Method	
					Size (nm)	Strain $\times 10^{-3}$
$Ca_9Y(PO_4)_7$	10.4377	37.2636	3516.16	70	91	6.5
$Ca_9Y(PO_4)_7$:0.01%Pr^{3+}	10.4393	37.3020	3520.50	68	94	7.8
$Ca_9Y(PO_4)_7$:0.1%Pr^{3+}	10.4415	37.3116	3522.88	67	99	7.3
$Ca_9Y(PO_4)_7$:0.5%Pr^{3+}	10.4462	37.3248	3527.30	66	100	7.4
$Ca_9Y(PO_4)_7$:1%Pr^{3+}	10.4472	37.3656	3531.82	72	103	7.1
$Ca_9Y(PO_4)_7$:1.5%Pr^{3+}	10.4483	37.3706	3533.06	74	105	5.9
$Ca_9Y(PO_4)_7$:2%Pr^{3+}	10.4553	37.381	3538.76	77	106	5.4

According to the diffraction data, the size of the crystallites (D) was estimated using the Scherrer equation [41]:

$$D = K\lambda / \beta \cos\theta \quad (1)$$

where K is the shape constant equal to 0.9, λ is the wavelength of the incident X-ray (1.54056 Å), θ is the Bragg angle, and β is the Full Width at Half Maximum (FWHM) of

the diffraction peak. The crystallite size of the $Ca_9Y_{1-x}Pr_x(PO_4)_7$ samples, estimated by the Scherrer formula, does not depend on the concentration of the activator (Table 1). Since the crystallite size can be affected by lattice deformation and lattice defects, the size and the strain were estimated using the Williamson–Hall (W–H) plot method [42,43] according to the following formula:

$$\beta hkl * \cos\theta = \frac{k\lambda}{D} + 4\varepsilon * \sin\theta \quad (2)$$

where ε is the strain. Linear fitting of dates obtained by plotting $\beta\cos\theta$ (x-axis) and $4\varepsilon\sin\theta$ (y-axis) was used to estimate crystallite size from y-axis intersections and strain from slope (Figure S1). The strains and the crystallite size values are included in Table 1. Measurements by the W–H methods revealed that the crystallite size of the powders increases continuously with increasing Pr^{3+} concentration. It should be noted that the crystallite sizes calculated using the Scherrer method are somewhat smaller than those calculated from the W–H plot method. This can be explained by the fact that the Scherrer method does not take into account any particle agglomerations.

2.2. Optical Characterization

The refractive index of CYPO crystal together with the energy bandgap E_g, was estimated using the method based on the chemical formula [44,45]. Calculated results are as follows: the refractive index n = 1.67 and E_g between 6.22 and 6.55 eV. The obtained relatively high value of E_g makes this crystal suitable for applications, especially as a phosphor in the UV range.

Absorption spectra of the investigated polycrystals doped with Pr^{3+} ions show the absorption peaks characteristic of the used dopants. Figure S2 shows transitions from the ground $^3H_4$ energy level to the next excited states of the praseodymium(III). The center of gravity of the $^1D_2$ absorption level is at 596 nm (16,779 cm^{-1}), with the whole band ranging from about 570 to 620 nm, with a maximum observed at 591 nm (16,920 cm^{-1}).

2.3. Phonon Properties

The primitive unit cell of the $Ca_9Y(PO_4)_7$ *R3c* structure is composed of 90 atoms having 270 degrees of freedom ($45A_1 + 45A_2 + 90E$). According to the factor group analysis, 267 of them ($45A_1 + 45A_2 + 90E$) are optical modes, whereas 3 are acoustic ones ($A_1 + E$). Because the $45A_2$ modes are silent and the structure is polar, the remaining $44A_1$ and 89E symmetry modes are both IR- and Raman-active. As a result, 133 IR and Raman bands are expected.

Figure 3 demonstrates the IR transmittance and Raman spectra measured for the representative sample containing 1 mol% of Pr^{3+} ions. The registered spectra are very similar to previously reported data for the $Ca_9Y(PO_4)_7$ *R3c* structure and other similar compounds, i.e., $Ca_9Bi(PO_4)_7$ [46], $Ca_9RE(PO_4)_7$ (RE = La, Pr, Nd, Eu, Gd, Dy, Tm, Yb) [47], and $Ca_9Y(PO_4)_{7(1-x)}(VO_4)_{7x}$ [48]. The Raman spectrum of undoped $Ca_9Y(PO_4)_7$, previously reported by Zhang et al., shows the presence of Raman bands at 404, 440, 610, 945, and 971 cm^{-1} [48]. Our studies indicate that the corresponding Raman bands are upshifted by 1–3 cm^{-1}, which can be attributed to different methods of synthesis and/or the presence of heavier Pr^{3+} ions. The IR spectrum of $Ca_9Y(PO_4)_7$, to the best of our knowledge, has not been reported so far.

All the observed IR and Raman bands can be divided into internal vibrations associated with phosphate ions and lattice modes. Based on the literature data [47,49,50], they were assigned as follows: 377–557 cm^{-1} to the symmetric bending modes (δ_a), 590–636 cm^{-1} to the antisymmetric bending modes (δ_{as}), 925–973 cm^{-1} to the symmetric stretching modes (ν_s), and 1001–1125 cm^{-1} to the antisymmetric stretching modes (δ_{as}) of the deformed tetrahedral phosphate ions. All Raman bands below 332 cm^{-1} were assigned to the lattice modes, which included the translational and vibrational modes of orthophosphate ions, as well as translations of Ca^{2+} and Y^{3+}/Pr^{3+}.

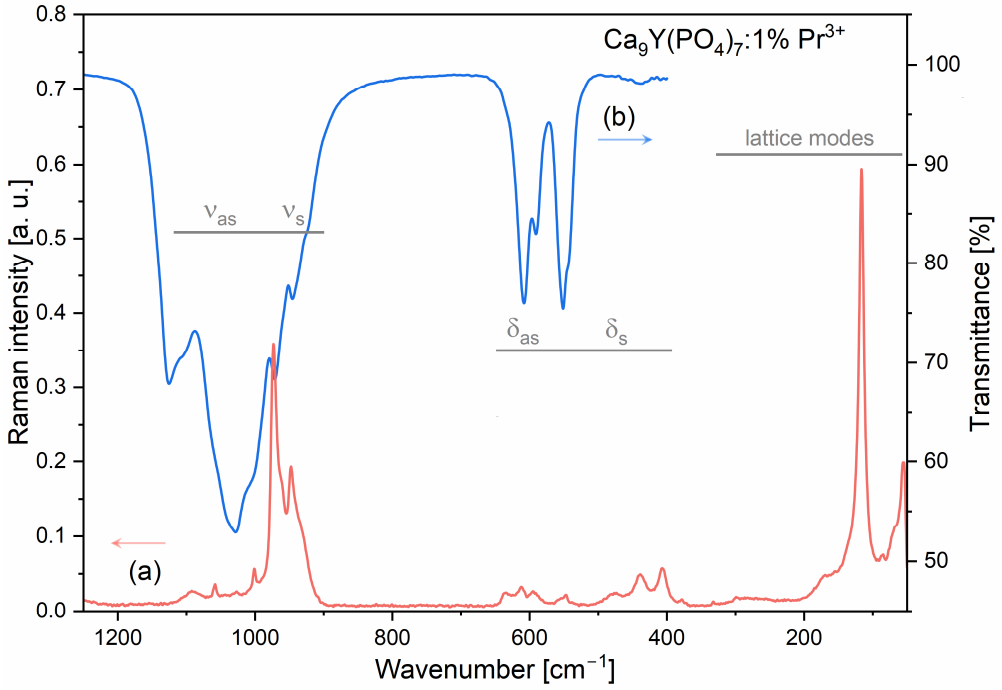

Figure 3. Raman (**a**) and IR (**b**) spectra of the $Ca_9Y(PO_4)_7$ sample doped with 1 mol% of Pr^{3+} ions.

2.4. Emission in the UVC Range

Measurements in the UVC range were carried out using a deuterium lamp and the McPherson spectrometer. Figure 4 and Figure S3 present the excitation and emission spectra of CYPO:0.5%Pr^{3+} polycrystals, which correspond to the $4f^2 \leftrightarrow 4f^15d^1$ interconfigurational optical transitions.

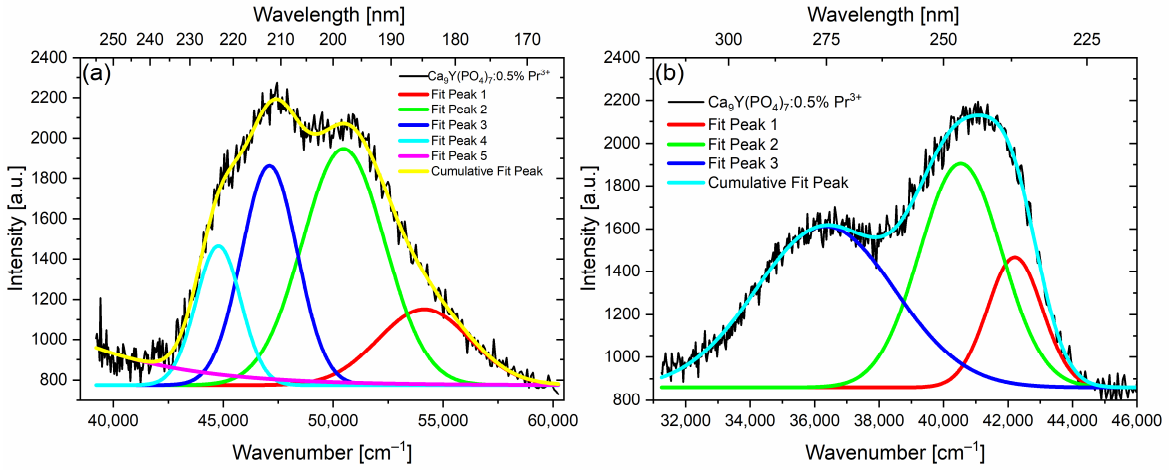

Figure 4. The room temperature excitation (**a**) and emission (**b**) spectra of CYPO:0.5% Pr^{3+} polycrystals. The spectra are fitted to a sum of Gaussian bands.

The excitation band monitored at 275 nm decomposed into the sum of Gaussian bands centered at 54,146 cm^{-1}, 50,473 cm^{-1}, 47,103 cm^{-1}, and 44,782 cm^{-1} (Figure 4a). The emission spectra excited at 196 nm were deconvoluted into Gaussian components centered at 42,221 cm^{-1}, 40,532 cm^{-1}, and 36,331 cm^{-1} (Figure 4b). Based on the excitation and emission spectra, the Stokes shift (ΔS) was estimated by comparing the position of the lowest energy absorption maxima and the position of the highest energy emission maxima. The Stokes shift calculated for CYPO:0.5% Pr^{3+} polycrystals is 2561 cm^{-1}. Notably, this value is nearly 1000 cm^{-1} larger than the Stokes shift reported for the $Ca_9Y(PO_4)_7$:1% Pr^{3+}

sample in the work of [17]. This is mainly caused by differences in the excitation spectrum, which for that publication is slightly wider in the lower energy range. The observed difference may be due to the differences in the sample synthesis and spectrophotometer sensitivity. Another explanation may be due to different crystallite sizes, given the difference in annealing temperatures between samples. According to this [17] work, efficient Pr^{3+} interconfigurational emission transitions of this compound may also be due to the fact that the Stokes shift is (like in our case) less than about 3300 cm^{-1}, the $4f^15d^1$-$4f^2$ radiative transition dominates over the nonradiative relaxation from the $4f^15d^1$ to the $4f^2$ levels of Pr^{3+} ions [16,17].

Interconfigurational transitions are allowed by Laporte's selection rule [51–53] and in this case, in the comparison to the result of the luminescence decay times, the luminescence intensity increases with the addition of Pr^{3+}, so that the number of emission centers responsible for this luminescence increases. The obtained emission in the UVC range is well matched to the radiation, which is characterized by disinfecting properties, eliminating viruses and bacteria.

Figure 5 reveals the presence of at least two distinct Pr^{3+} sites. Excitation of $Ca_9Y_{0.995}Pr_{0.005}(PO_4)_7$ at shorter wavelengths, specifically 196 nm, activates all Pr^{3+} ions in the host, while excitation of $Ca_9Y_{0.99}Pr_{0.01}(PO_4)_7$ at 230 nm selectively activates only one class of Pr^{3+} ions located at the site with a stronger crystal field. The spectrum obtained with the former excitation demonstrates not only strong $4f^15d^1 \rightarrow {}^3H_J + {}^3F_{2,3}$ transitions observed between 220 and 320 nm, but also relatively strong $4f^15d^1 \rightarrow {}^3P_J$ transition with the peak at 403 nm. Since the ${}^3P_J$ term is radiatively excited, transitions to ${}^3H_4$ from ${}^3P_0$ and ${}^3P_1$ are also observed. However, under 230 nm excitation, the 4f→4f emission is notably weak, indicating minimal energy transfer from the 5d to 4f electronic configuration. This characteristic is attributed to the low value of the Stokes shift [17], which in our case amounts to 2561 cm^{-1}.

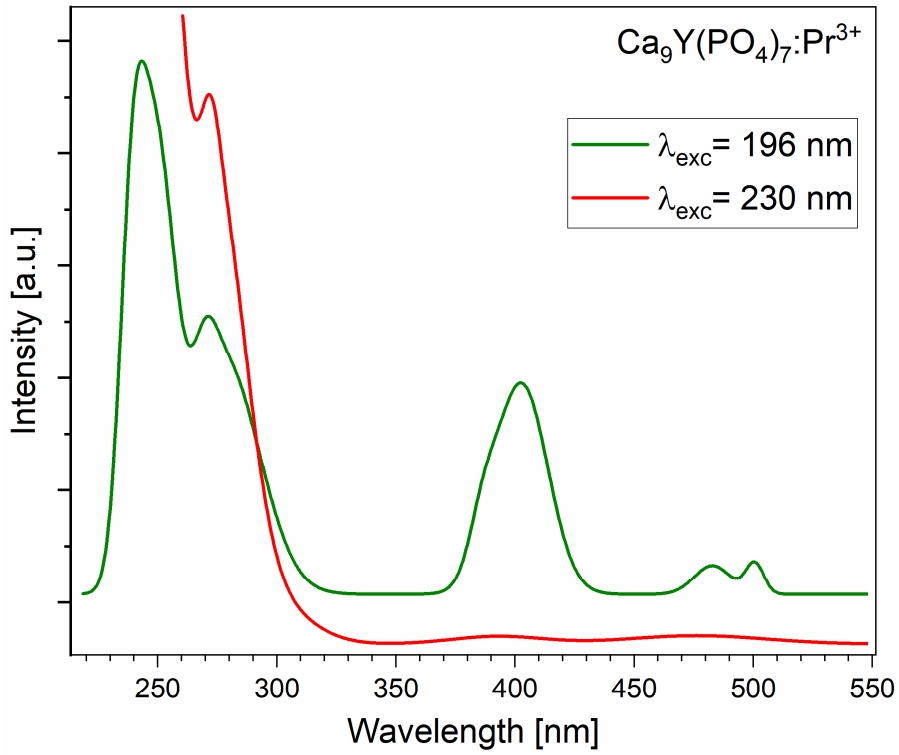

Figure 5. The UVC emission spectrum of $Ca_9Y_{1-x}Pr_x(PO_4)_7$ polycrystals, at 300 K.

Since the 5d bands are within the range of blue light excitation, upconversion into ultraviolet radiation was observed. The influence of the excitation power "P" of the diode laser (444 nm) on the luminescence intensity "I" of the 5d-4f band in the UVC range was

investigated. Detailed data are marked in Figure 6a. The characteristic in the log/log scale is linear and is proportional to $I \sim P^n$, where n is the number of pump photons required to excite the emitting level [54]. The obtained result of $n = 2$ suggests that two photons are involved in the upconversion process. Figure 6b presents this anti-Stokes emission spectrum, with laser excitation at 444 nm. The results obtained after integrating the emission area show that most (about 72%) of the obtained UV upconversion emission is in the UVC range. The UVB part, which is less harmful to the viruses, possesses only 28% of the area in the emission spectrum.

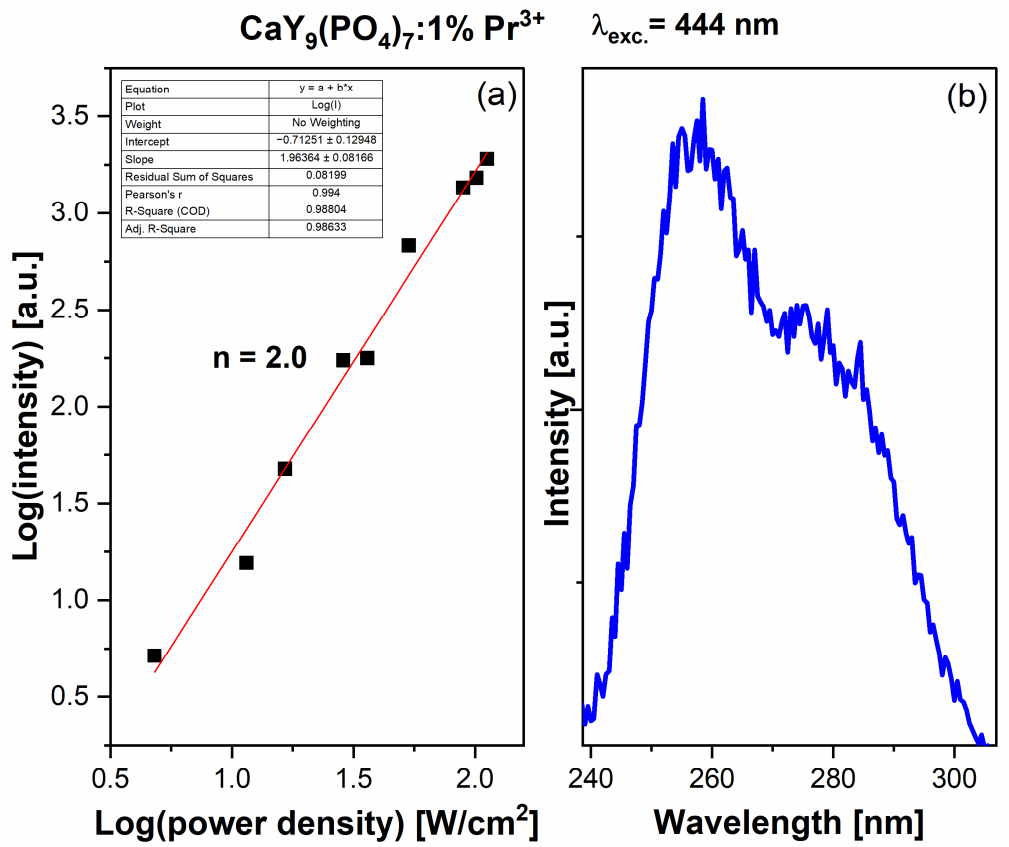

Figure 6. (**a**) Power density (per unit area) dependence of the upconversion emission of $Ca_9Y_{0.99}Pr_{0.01}(PO_4)_7$ polycrystals; (**b**) The anti-Stokes emission spectra of $Ca_9Y_{0.99}Pr_{0.01}(PO_4)_7$ polycrystals in the UVC range.

For the CYPO powders studied, measurements of luminescence intensity "I" of upconversion and Stokes emissions were performed as a function of Pr^{3+} concentration "X" (see Figure 7). The intensity of emission could be approximated with such a function $I \sim X^a$, where "a" is the value of an exponent. For initial Pr^{3+} concentrations (for which so-called concentration quenching does not occur), the UVC upconversion emission was fitted with a quadratic function, while the Stokes emission depends linearly on the Pr^{3+} concentration there (see inset in Figure 7). The quadratic dependence of UVC emission intensity on Pr^{3+} concentration indicates the process of energy transfer upconversion (ETU) [54], which occurs in pairs of Pr^{3+} ions. Please note that for low concentrations, e.g., 0.5% Pr^{3+} the intensity of upconversion emission is relatively low compared to Stokes luminescence. On the other hand, a sample with a praseodymium ion concentration of 2% has a much weaker Stokes emission (about 20% compared to the most intense sample), while the anti-Stokes emission in the UVC region, although weaker, possesses a 60% intensity of the best CYPO sample (see Figure 7).

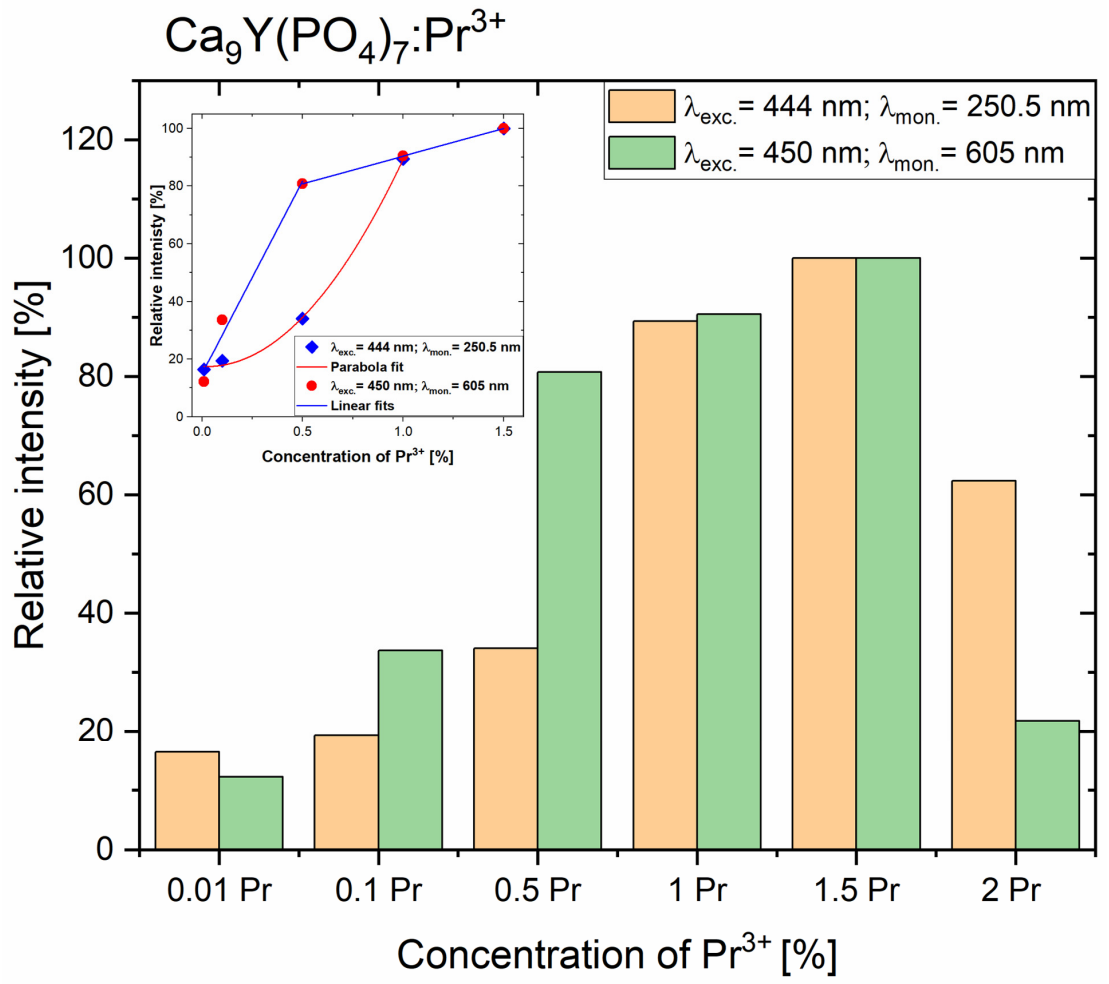

Figure 7. Relative intensities of the UVC upconversion and Stokes emissions of $Ca_9Y(PO_4)_7$ polycrystals, for different concentrations of the doped Pr^{3+} ions. Inset shows the fitted intensity of these emissions.

2.5. Spectroscopic Properties in the Visible Range

Figure 8 shows both, the excitation and luminescence spectra of CYPO polycrystals doped with Pr^{3+} ions. The most intense emission comes from the transition from level $^1D_2$. The excitation spectrum in the UVC range, when monitoring the $^1D_2 \rightarrow {}^3H_4$ transition, was very weak. Three peaks from the transition $^3P_0 \rightarrow {}^3H_4$ are observed. The most intense is the red luminescence $^1D_2 \rightarrow {}^3H_4$ and for it, the greatest influence of temperature change is observed. A small emission peak at 530 nm comes from a transition from the $^3P_1$ level, because this level can be populated at room temperature with electrons from the neighboring $^3P_0$ emitting level. The shape of the excitation and luminescence bands is like the emission of Pr^{3+} ions in similar calcium phosphates, where instead of yttrium (as in this case), aluminum and lutetium ions were present in the crystal matrix [34].

The mechanisms of excitation, luminescence, as well as concentration quenching by cross-relaxation (CR) are as follows. When excitation by a laser diode or xenon lamp by energy matched to the $^3P_2$ praseodymium level, non-radiative transfer of the excitation energy to the $^3P_0$ and $^1D_2$ emitting levels occurs. Then, the emission from these levels to the ground state $^3H_4$ and higher excited states take place. The observed luminescence is also quenched by a non-radiative cross-relaxation process that occurs in ion pairs when ions are close enough to each other according to the following schemes: $[^1D_2, {}^3H_4] \rightarrow [^1G_4, {}^3F_4]$. When excited in the $^3P_2$ band, the energy is transferred non-radiatively to the nearby $^3P_0$ level, from which luminescence occurs. On the other hand, the emission from the

$^1D_2$ level can be populated from the $^3P_0$ level by multi-phonon relaxation due to the high energy of the phonons in the phosphate matrices of around 1200 cm^{-1} [32].

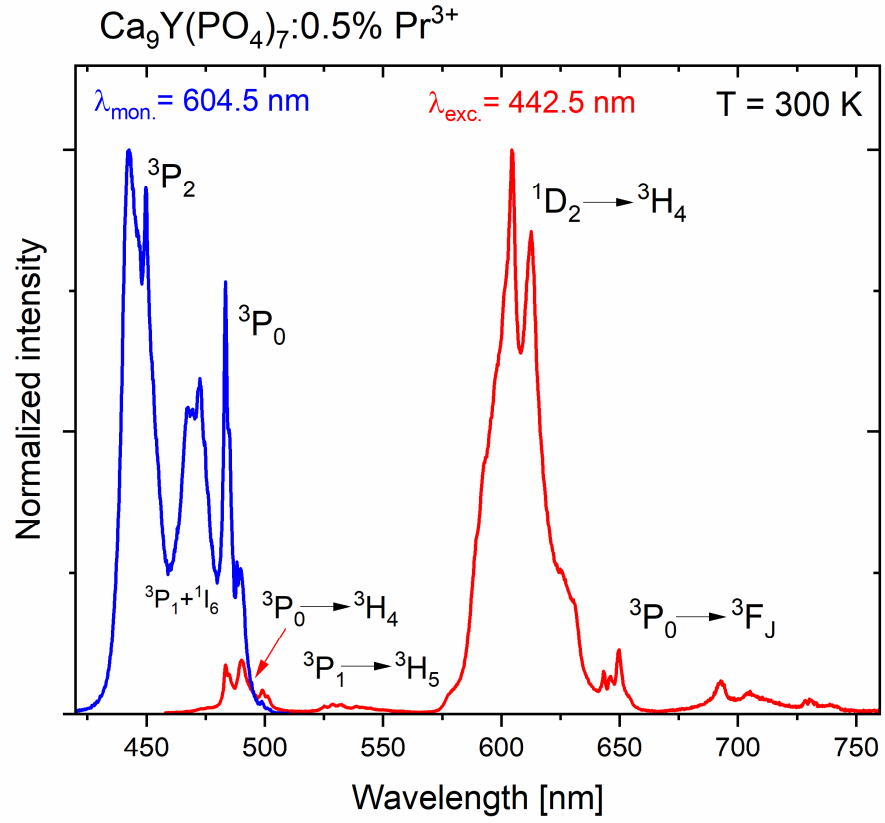

Figure 8. Excitation and emission spectra of $Ca_9Y_{0.995}Pr_{0.005}(PO_4)_7$ polycrystals.

The energy bandgap law states that if the difference between two energy levels is greater than five times the value of the highest energy phonon in the host medium, the probability of multiphonon relaxation will be negligible. The multiphonon non-radiative transition rates "W_{NR}" can be written using the formula [55,56]:

$$W_{NR} = (1/t_0)\exp(-ap), \quad (3)$$

where $p = \Delta E/h\upsilon_{max}$ is the number of phonons needed to overcome the ΔE gap, h is the Plank constant, υ_{max} is the highest phonon frequency in the host, and t_0 and a are the empirically fitted parameters. The absorption spectrum shows that the energy distance between the $^3P_0$ and $^1D_2$ levels is less than 4000 cm^{-1}; therefore, in the case of this host as well as other phosphates, since $p \approx 3$, the probability of multiphonon relaxation will be significant. The cross-relaxation process [$^3P_0$, $^3H_4$] → [$^3H_6$, $^1D_2$] could also populate the $^1D_2$ level but is much weaker than those from $^1D_2$ because, according to the selection rule, they are spin-forbidden.

The luminescence intensity of the 4f emission decreases with increasing temperature, but it is a slow decrease and stable in the range of temperatures measured up to 540 °C. For the temperature of 150 °C, this intensity is almost 80%, while 50% of the room temperature intensity is visible for the sample only at the temperature of 420 °C, i.e., 693 K (see Figures S4 and S5 in the Supplementary Materials). This proves the very good temperature stability of the measured sample.

The luminescence decay times of the 4f emission are not monoexponential. However, the luminescence decay curve has a similar structure to a single-exponential function, which may indicate, on the one hand, the dominant influence of one of the sites (crystallographic positions), as well as the fact that the doped ions, located mainly in three different

crystallographic positions, possess similar luminescence lifetimes (see Figure 9). The integral equation:

$$\tau = \frac{\int I \cdot t \, dt}{\int I \, dt} \quad (4)$$

was used to calculate the mean value of the luminescence lifetime; thus, all components of the decay curve were averaged. The decay times of the luminescence from the $^1D_2$ level to the $^3H_4$ state are spin-forbidden; therefore, they are much longer than the decay times from the $^3P_0$ level (see results in Table 2).

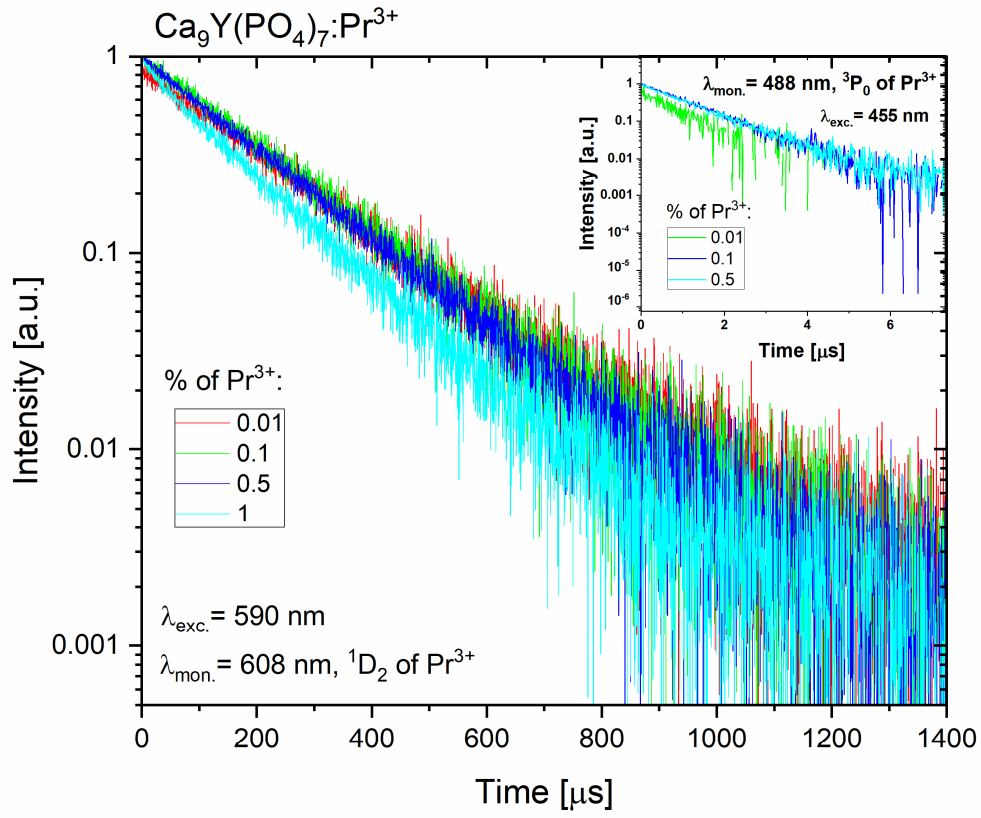

Figure 9. The luminescence decay curves of the emitting levels of Pr^{3+} ions in $Ca_9Y(PO_4)_7$ polycrystals.

Table 2. Luminescence lifetimes for Pr^{3+} ions in $Ca_9Y(PO_4)_7$ matrices.

Sample	Lifetime [μs]	
	$^3P_0$ (Pr^{3+})	$^1D_2$ (Pr^{3+})
$Ca_9Y(PO_4)_7$:0.01% Pr^{3+}	1	211
$Ca_9Y(PO_4)_7$:0.1% Pr^{3+}	1	197
$Ca_9Y(PO_4)_7$:0.5% Pr^{3+}	0.9	187
$Ca_9Y(PO_4)_7$:1% Pr^{3+}	0.6	151

Concentration quenching is observed quite quickly for Pr^{3+} ions. A slight reduction in the luminescence decay time from the $^3P_0$ level is visible from the concentration of 0.5% Pr^{3+}, while a slight decrease in the length of the emission decay time for the $^1D_2$ level begins quicker, where this effect is visible also for concentration lower than 0.5%, and it is very clear for the 1% of Pr^{3+}. For the measured calcium phosphate polycrystals, the cross-relaxation process, as mentioned above, quenches the luminescence, and the multiphonon relaxation from the $^1D_2$ level is less effective since the energy distance the lower $^1G_4$ is above 7000 cm^{-1} and overt than five phonons must be involved.

3. Experimental

3.1. Synthesis

$Ca_9Y_{1-x}Pr_x(PO_4)_7$ polycrystals with the concentration of Pr^{3+} (0.01; 0.1; 0.5; 1.0; 1.5; 2.0 mol%) were synthesized by solid-state reaction technique. The reagents $CaCO_3$ (99.95%, Alfa Aesar, Haverhill, MA, USA), Y_2O_3 (99.99%, Acroc Organics, Geel, Belgium), Pr_2O_3 (99.9%, Chem PUR, Karlsruhe, Germany), $NH_4H_2PO_4$ (99.999%, Acros Organics) were used as precursors. All precursors were weighed in the required proportion, placed in an agate mortar, and thoroughly ground. Then, annealing was carried out at a temperature of 700 °C for 2 h and then at a temperature of 1100 °C for 4 h. After each stage of annealing, the sample was ground again in an agate mortar.

3.2. Measurements

The X-ray powder diffraction (XRD) measurements were performed using an X'Pert PRO X-ray diffractometer (Panalytical, Malvern, UK). The reflectance absorption spectra were recorded using a Cary 5000 UV-VIS-NIR spectrophotometer. Pure Al_2O_3 powder was used as the baseline for spectrum correction. The excitation and emission spectra were measured using an FLS1000 fluorescence spectrometer from Edinburgh Instruments (Livingston, UK) equipped with a 450 W xenon lamp.

For the measurement of emission spectra, while using a xenon lamp with an excitation wavelength at 230 nm, the CYPO:Pr^{3+} polycrystalline powder was placed in a special holder with lithium fluoride (LiF) glass, which has high transparency in this area, and is better suited for measurements in the UVC range than a quartz tube, which may interfere with the measurement results of samples. The spectra taken using an FLS1000 spectrometer were automatically corrected to avoid the influence of the monochromator efficiency and the spectral response of the detector. For the temperature-dependent emission spectra, the Hamamatsu PMA-12 detector with Linkam THMS 600 Heating/Freezing Stage and laser diode at 450 nm were used. Decay time profiles were provided by using a Continuum Surelite I Optical Parametric Oscillator (OPO) pumped with a Nd:YAG laser. The UVC measurements were performed using a VUV McPherson spectrometer (McPherson, Chelmsford, MA, USA) equipped with a Czerny–Turner monochromator and a 150 W deuterium lamp. The upconversion emission was recorded on the McPherson spectrometer, using the excitation laser line at 444 nm focused on the area of 0.75 mm^2 and corrected for the used filter characteristics.

The Raman spectrum was collected with a Renishaw inVia Raman spectrometer (Renishaw, Wotton-under-Edge, UK) equipped with a confocal DM2500 Leica optical microscope and an Ar-ion laser operating at 514.5 nm. The mid-IR ATR (attenuated total reflection) spectrum was measured using a Nicolet iS50 FT-IR spectrometer (Thermo Fisher Scientific, Waltham, MA, USA) equipped with an ATR accessory with a diamond crystal.

4. Conclusions

$Ca_9Y(PO_4)_7$ has proven to be an excellent UVC phosphor when excited via the 5d bands, but it was also shown that despite the relatively short lifetime of the $^3P_0$ level. It is likewise possible to obtain UVC emission when excited with blue light. According to our knowledge, this is the first paper describing the results of the UVC upconversion emission for this compound doped with the praseodymium(III) ions. The crystalline structures have been confirmed with the XRD measurement. The average crystallite sizes are in the nanoscale. Investigation in absorption, excitation, IR transmittance, Raman, and emission spectra, as well as the emission decay time profiles, were presented. Spectroscopic properties depend on the percent of doped rare-earth ions. The Pr^{3+} main luminescence of the 4f electronic configuration comes from the $^1D_2$ multiplets. A shortening of luminescence decay times with increasing concentrations of Pr^{3+} doped ions was noticed. The emission wavelength range, predominantly falling within the UVC limit, coupled with the minimal emission intensity in the visible range upon direct excitation of the $4f^15d^1$ Pr^{3+} levels, renders this material a promising UVC phosphor. Consequently, further investiga-

tion into CYPO: Pr^{3+} as a scintillator for combating X-ray-resistant tumors is warranted. The future paths of our investigation will be focused on X-ray excitation of the modified CYPO host by exchange of Y with a heavier element like Lu, which will ensure a higher absorption cross-section.

However, the observed anti-Stokes emission in CYPO: Pr^{3+} appears to be less efficient compared to other established upconverters such as Y_2SiO_5: Pr^{3+}, for example. It is possible that additional modifications to the synthesis and sample composition by exchange of the host cations may enhance the upconversion effect.

Supplementary Materials: The following supporting information can be downloaded at: https://www.mdpi.com/article/10.3390/molecules29092084/s1, Table S1: Distances between yttrium sites and oxygen ligands in $Ca_9Y(PO_4)_7$; Figure S1: Plots of $\beta\cos\theta$ versus $4\sin\theta$ for $Ca_9Y_{1-x}Pr_x(PO_4)_7$ ($0 \leq x \leq 0.02$) nanoparticles; Figure S2: Absorption spectra of $Ca_9Y_{0.085}Pr_{0.015}(PO_4)_7$; Figure S3: Excitation and emission spectra of $Ca_9Y_{0.995}Pr_{0.005}(PO_4)_7$ polycrystals in the UVC range; Figure S4: Visualization of the temperature dependence luminescence intensity of $Ca_9Y_{0.995}Pr_{0.005}(PO_4)_7$ for the selected temperatures; Figure S5: Quenching of the luminescence intensity of $Ca_9Y_{0.995}Pr_{0.005}(PO_4)_7$ in a function of temperature.

Author Contributions: Conceptualization, P.J.D. and K.L.; methodology, K.L., N.R., O.B., R.L. and P.Z.; validation, P.J.D., K.L. and N.R.; formal analysis, K.L., P.J.D. and N.R.; investigation, K.L., N.R., R.L., P.Z. and P.J.D.; resources, O.B., N.R. and P.J.D.; data curation, P.J.D. and K.L.; writing—original draft preparation, K.L., N.R. and P.J.D.; writing—review and editing, K.L., P.J.D., N.R., O.B. and P.Z; visualization, K.L., N.R. and P.Z.; supervision, P.J.D. and K.L.; project administration, P.J.D. and K.L.; funding acquisition, P.J.D. All authors have read and agreed to the published version of the manuscript.

Funding: This research was funded by the National Science Centre (Poland), project OPUS number: 2021/41/B/ST5/03792.

Institutional Review Board Statement: Not applicable.

Informed Consent Statement: Not applicable.

Data Availability Statement: Data are contained within the article.

Conflicts of Interest: The authors declare no conflicts of interest.

References

1. Cates, E.L.; Wilkinson, A.P.; Kim, J.-H. Visible-to-UVC upconversion efficiency and mechanisms of $Lu_7O_6F_9$:Pr^{3+} and Y_2SiO_5:Pr^{3+} ceramics. *J. Lumin.* **2015**, *160*, 202–209. [CrossRef]
2. Kowalski, W. UV Surface Disinfection. In *Ultraviolet Germicidal Irradiation Handbook: UVGI for Air and Surface Disinfection*; Kowalski, W., Ed.; Springer: Berlin/Heidelberg, Germany, 2009; pp. 233–254. [CrossRef]
3. Yang, J.-H.; Wu, U.-I.; Tai, H.-M.; Sheng, W.-H. Effectiveness of an ultraviolet-C disinfection system for reduction of healthcare-associated pathogens. *J. Microbiol. Immunol. Infect.* **2019**, *52*, 487–493. [CrossRef]
4. Browne, K. Brought to Light: How Ultraviolet Disinfection Can Prevent the Nosocomial Transmission of COVID-19 and Other Infectious Diseases. *Appl. Microbiol.* **2021**, *1*, 537–556. [CrossRef]
5. Rutala, W.A.; Donskey, C.J.; Weber, D.J. Disinfection and sterilization: New technologies. *Am. J. Infect. Control* **2023**, *51*, A13–A21. [CrossRef]
6. Ramakrishna, G.; Nagabhushana, H.; Basavaraj, R.B.; Naik, R.; Sharma, S.C.; Prasad, B.D.; Premkumar, H.B.; Anantharaju, K.S.; Prashantha, S.C. Calotropis gigantean-assisted YSO:Pr^{3+} nanophosphors: Near-ultraviolet (NUV) photoluminescence and J-O analysis for solid-state lighting solutions. *Inorg. Nano-Met. Chem.* **2017**, *47*, 1234–1242. [CrossRef]
7. Drozdowski, W.; Dorenbos, P.; Drozdowska, R.; Bos, A.J.J.; Poolton, N.R.J.; Tonelli, M.; Alshourbagy, M. Effect of Electron Traps on Scintillation of Praseodymium Activated $Lu_3Al_5O_{12}$. *IEEE Trans. Nucl. Sci.* **2009**, *56*, 320–327. [CrossRef]
8. Srivastava, A.M. Aspects of Pr^{3+} luminescence in solids. *J. Lumin.* **2016**, *169*, 445–449. [CrossRef]
9. Ozen, G.; Collins, J.; Bettinelli, M.; Di Bartolo, B. Luminescence of $Y_3AL_5O_{12}$ nano-particles doped with praseodymium ions. *Opt. Mater.* **2013**, *35*, 1360–1365. [CrossRef]
10. Manzani, D.; Pabœuf, D.; Ribeiro, S.J.L.; Goldner, P.; Bretenaker, F. Orange emission in Pr^{3+}-doped fluoroindate glasses. *Opt. Mater.* **2013**, *35*, 383–386. [CrossRef]
11. Runowski, M.; Woźny, P.; Martín, I.R.; Lavín, V.; Lis, S. Praseodymium doped YF_3:Pr^{3+} nanoparticles as optical thermometer based on luminescence intensity ratio (LIR)—Studies in visible and NIR range. *J. Lumin.* **2019**, *214*, 116571. [CrossRef]

12. Dereń, P.J.; Lemański, K. On tuning the spectroscopic properties of $LaAlO_3$:Pr^{3+} nanocrystallites. *J. Lumin.* **2011**, *131*, 445–448. [CrossRef]
13. Lemański, K.; Dereń, P.J. Luminescent properties of $LaAlO_3$ nanocrystals, doped with Pr^{3+} and Yb^{3+} ions. *J. Lumin.* **2014**, *146*, 239–242. [CrossRef]
14. Lemański, K.; Bondzior, B.; Szymański, D.; Dereń, P.J. Spectroscopic properties of $Gd_xLa_{1-x}AlO_3$ nanocrystals doped with Pr^{3+} ions. *New J. Chem.* **2019**, *43*, 6242–6248. [CrossRef]
15. Srivastava, A.M.; Setlur, A.A.; Comanzo, H.A.; Hannah, M.E.; Schmidt, P.A.; Happek, U. Luminescence from the Pr^{3+} $4f^15d^1$ and $^1S0$ states in $LiLaP_4O_{12}$. *J. Lumin.* **2009**, *129*, 126–129. [CrossRef]
16. Srivastava, A.M.; Jennings, M.; Collins, J. The interconfigurational ($4f^15d^1 \rightarrow 4f^2$) luminescence of Pr^{3+} in $LuPO_4$, $K_3Lu(PO_4)_2$ and $LiLuSiO_4$. *Opt. Mater.* **2012**, *34*, 1347–1352. [CrossRef]
17. Camardello, S.J.; Toscano, P.J.; Srivastava, A.M. ON the interconfigurational $4f^n \leftrightarrow 4f^{n-1}$ $5d^1$ optical transitions of Ce^{3+} and Pr^{3+} in $Ca_9R^{3+}(PO_4)_7$[R^{3+} = Al, Ga, Sc, Lu, Y, Gd, La]. *J. Lumin.* **2016**, *176*, 363–366. [CrossRef]
18. Acton, Q.A. *Phosphates—Advances in Research and Application: 2013 Edition*; ScholarlyEditions: Atlanta, GA, USA, 2013; Available online: https://books.google.pl/books?id=1EudM1a_RJkC (accessed on 8 January 2024).
19. Dorozhkin, S.V.; Epple, M. Biological and Medical Significance of Calcium Phosphates. *Angew. Chem. Int. Ed.* **2002**, *41*, 3130–3146. [CrossRef]
20. Woyengo, T.A.; Nørgaard, J.V.; van der Heide, M.E.; Nielsen, T.S. Calcium and phosphorus digestibility in rock- and bone-derived calcium phosphates for pigs and poultry: A review. *Anim. Feed Sci. Technol.* **2022**, *294*, 115509. [CrossRef]
21. Eliaz, N.; Metoki, N. Calcium Phosphate Bioceramics: A Review of Their History, Structure, Properties, Coating Technologies and Biomedical Applications. *Materials* **2017**, *10*, 334. [CrossRef]
22. Canillas, M.; Pena, P.; de Aza, A.H.; Rodríguez, M.A. Calcium phosphates for biomedical applications. *Boletín Soc. Española Cerámica Vidr.* **2017**, *56*, 91–112. [CrossRef]
23. Kalbarczyk, M.; Szcześ, A. Potential biomedical application of calcium phosphates obtained using eggshells as a biosource of calcium at different initial pH values. *Ceram. Int.* **2021**, *47*, 33687–33696. [CrossRef]
24. Lima, F.; Fernandes, J.; Oliveira, E.; Fronzaglia, G.; Kahn, H. Laboratory evaluations of feed-grade and agricultural-grade phosphates. *Poult. Sci.* **1999**, *78*, 1717–1728. [CrossRef]
25. Lima, F.R.; Mendonça, C.X.; Alvarez, J.C.; Ratti, G.; Lenharo, S.L.R.; Kahn, H.; Garzillo, J.M.F. Chemical and Physical Evaluations of Commercial Dicalcium Phosphates as Sources of Phosphorus in Animal Nutrition. *Poult. Sci.* **1995**, *74*, 1659–1670. [CrossRef]
26. Habraken, W.; Habibovic, P.; Epple, M.; Bohner, M. Calcium phosphates in biomedical applications: Materials for the future? *Mater. Today* **2016**, *19*, 69–87. [CrossRef]
27. Dahiya, H.; Dalal, M.; Singh, A.; Siwach, A.; Dahiya, M.; Nain, S.; Taxak, V.B.; Khatkar, S.P.; Kumar, D. Spectroscopic characteristics of Eu^{3+}-activated $Ca_9Y(PO_4)_7$ nanophosphors in Judd–Ofelt framework. *Solid State Sci.* **2020**, *108*, 106341. [CrossRef]
28. Huang, C.-H.; Chen, T.-M.; Cheng, B.-M. Luminescence Investigation on Ultraviolet-Emitting Rare-Earth-Doped Phosphors Using Synchrotron Radiation. *Inorg. Chem.* **2011**, *50*, 6552–6556. [CrossRef]
29. Wu, X.; Liang, Y.; Chen, R.; Liu, M.; Cheng, Z. Photoluminescence properties of emission-tunable $Ca_9Y(PO_4)_7$: Tm^{3+}, Dy^{3+} phosphor for white light emitting diodes. *Mater. Chem. Phys.* **2011**, *129*, 1058–1062. [CrossRef]
30. Zhuang, Y.; Wang, D.; Yang, Z. Upconversion luminescence and optical thermometry based on non-thermally-coupled levels of $Ca_9Y(PO_4)_7$: Tm^{3+}, Yb^{3+} phosphor. *Opt. Mater.* **2022**, *126*, 112167. [CrossRef]
31. Górecka, N.; Szczodrowski, K.; Lazarowska, A.; Barzowska, J.; Michalik, D.; Grinberg, M. The influence of charge compensation defects on the spectroscopic properties of europium doped $Ca_9Y(PO_4)_7$. *RSC Adv.* **2017**, *7*, 40549–40557. [CrossRef]
32. Gao, G.; Turshatov, A.; Howard, I.A.; Busko, D.; Joseph, R.; Hudry, D.; Richards, B.S. Up-Conversion Fluorescent Labels for Plastic Recycling: A Review. *Adv. Sustain. Syst.* **2017**, *1*, 1600033. [CrossRef]
33. Ueda, K.; Oya, A.; Nagashima, S.; Ogata, T.; Honma, T.; Omata, T. Site-Dependent Luminescence from Pr^{3+} in Double-Perovskite-Type Alkaline Earth Lanthanum Tantalates. *J. Phys. Chem. C* **2023**, *127*, 8833–8839. [CrossRef]
34. Watras, A.; Carrasco, I.; Pazik, R.; Wiglusz, R.J.; Piccinelli, F.; Bettinelli, M.; Deren, P.J. Structural and spectroscopic features of $Ca_9M(PO_4)_7$ (M = Al^{3+}, Lu^{3+}) whitlockites doped with Pr^{3+} ions. *J. Alloys Compd.* **2016**, *672*, 45–51. [CrossRef]
35. Piccinelli, F.; Trevisani, M.; Plaisier, J.R.; Bettinelli, M. Structural study of Yb^{3+}, Eu^{3+} and Pr^{3+} doped $Ca_9Lu(PO_4)_7$. *J. Rare Earths* **2015**, *33*, 977–982. [CrossRef]
36. Sahu, M.K.; Mula, J. White light emitting thermally stable bismuth phosphate phosphor $Ca_3Bi(PO_4)_3$:Dy^{3+} for solid-state lighting applications. *J. Am. Ceram. Soc.* **2019**, *102*, 6087–6099. [CrossRef]
37. Pązik, R.; Zawisza, K.; Watras, A.; Maleszka-Bagińska, K.; Boutinaud, P.; Mahiou, R.; Dereń, P.J. Thermal quenching mechanisms of the Eu^{3+} luminescence in $Ca_9Al(PO_4)_7$ obtained by citric route. *Mater. Res. Bull.* **2013**, *48*, 337–342. [CrossRef]
38. Paterlini, V.; El Khouri, A.; Bettinelli, M.; Trucchi, D.M.; Capitelli, F. Spectroscopic and Structural Properties of β-Tricalcium Phosphates $Ca_9RE(PO_4)_7$ (RE = Nd, Gd, Dy). *Crystals* **2021**, *11*, 1269. [CrossRef]
39. Liu, S.; Liang, Y.; Zhu, Y.; Li, H.; Cai, Y.; Tu, D. Full visible spectra emission introduced by crystal-site engineering in β-$Ca_3(PO_4)_2$-type solid solution phosphors for high quality white light emitting diodes application. *Chem. Eng. J.* **2019**, *375*, 121976. [CrossRef]
40. Shannon, R.D. Revised Effective Ionic Radii and Systematic Studies of Interatomie Distances in Halides and Chaleogenides. *Acta Cryst.* **1976**, *32*, 751–767. [CrossRef]

41. Scherrer, P. Bestimmung der Grösse und der inneren Struktur von Kolloidteilchen mittels Röntgenstrahlen, Nachrichten von Der Gesellschaft Der Wissenschaften Zu Göttingen. *Math.-Phys. Kl.* **1918**, *1918*, 98–100.
42. Williamson, G.K.; Hall, W.H. X-ray line broadening from filed aluminium and wolfram. *Acta Metall.* **1953**, *1*, 22–31. [CrossRef]
43. Rebrova, N.; Zdeb, P.; Lemański, K.; Macalik, B.; Bezkrovnyi, O.; Dereń, P.J. Upconversion Luminescence Proper-ties of Pr^{3+}-Doped BaYF 5 Nanoparticles Prepared by Microwave Hydrothermal Method. *Inorg. Chem.* **2024**, *63*, 3028–3036. [CrossRef]
44. Lemański, K.; Walerczyk, W.; Dereń, P.J. Luminescent properties of europium ions in $CaAl_2SiO_6$. *J. Alloys Compd.* **2016**, *672*, 595–599. [CrossRef]
45. Watras, A.; Boutinaud, P.; Pązik, R.; Dereń, P.J. Luminescence—Structure relationships in $MYP_2O_7:Eu^{3+}$ (M=K, Rb, Cs). *J. Lumin.* **2016**, *175*, 249–254. [CrossRef]
46. Li, K.; Shang, M.; Zhang, Y.; Fan, J.; Lian, H.; Lin, J. Photoluminescence properties of single-component white-emitting $Ca_9Bi(PO_4)_7$: Ce^{3+}, Tb^{3+}, Mn^{2+} phosphors for UV LEDs. *J. Mater. Chem. C Mater.* **2015**, *3*, 7096–7104. [CrossRef]
47. Asmaa, E.K.; Mohammed, E.; Giancarlo, D.V.; Armida, S.; Rosanna, R.; Rossi, M.; Francesco, C. Synthesis, structure reTnement and vibrational spectroscopy of new rare-earth tricalcium phosphates $Ca_9RE(PO_4)_7$ (RE = La, Pr, Nd, Eu, Gd, Dy, Tm, Yb). *Ceram. Int.* **2017**, *43*, 15645–15653.
48. Zhang, Z.Z.; Zhang, F.; Li, G.Q.; Zhang, J.; Zhang, W.F. Red-emitting phosphor series: $Ca_9Y(PO_4)_{7(1-x)}(VO_4)_{7x}$: Eu^{3+}(x = 0−1) with improved luminescence thermal stability by anionic polyhedron substitution. *J. Mater. Sci. Mater. Electron.* **2019**, *30*, 8838–8846. [CrossRef]
49. Godlewska, P.; Matraszek, A.; Macalik, L.; Hermanowicz, K.; Ptak, M.; Tomaszewski, P.E.; Hanuza, J.; Szczygieł, I. Spectroscopic and structural properties of $Na_3RE(PO_4)_2$:Yb orthophosphates synthesised by hydrothermal method (RE = Y, Gd). *J. Alloys Compd.* **2015**, *628*, 199–207. [CrossRef]
50. Kizalaite, A.; Grigoraviciute-Puroniene, I.; Asuigui, D.R.C.; Stoll, S.L.; Cho, S.H.; Sekino, T.; Kareiva, A.; Zarkov, A. Dissolution–precipitation synthesis and characterization of zinc whitlockite with variable metal content. *ACS Biomater. Sci. Eng.* **2021**, *7*, 3586–3593. [CrossRef] [PubMed]
51. Laporte, O.; Meggers, W.F. Some Rules of Spectral Structure*. *J. Opt. Soc. Am.* **1925**, *11*, 459–463. [CrossRef]
52. Walsh, B.M. Judd-Ofelt theory: Principles and practices. In *Advances in Spectroscopy for Lasers and Sensing*; Springer: Berlin/Heidelberg, Germany, 2006; pp. 403–433.
53. Bünzli, J.G. Rising Stars in Science and Technology: Luminescent Lanthanide Materials. *Eur. J. Inorg. Chem.* **2017**, *2017*, 5058–5063. [CrossRef]
54. Pollnau, M.; Gamelin, D.R.; Lüthi, S.R.; Güdel, H.U.; Hehlen, M.P. Power dependence of upconversion luminescence in lanthanide and transition-metal-ion systems. *Phys. Rev. B* **2000**, *61*, 3337–3346. [CrossRef]
55. Weber, M.J. Multiphonon Relaxation of Rare-Earth Ions in Yttrium Orthoaluminate. *Phys. Rev. B* **1973**, *8*, 54–64. [CrossRef]
56. Payne, S.A.; Bibeau, C. Picosecond nonradiative processes in neodymium-doped crystals and glasses. *J. Lumin.* **1998**, *79*, 143–159. [CrossRef]